Fall 2021

A compact wavelength meter using a multimode fiber

Ogbole Collins Inalegwu

Department:

A COMPACT WAVELENGTH METER USING A MULTIMODE FIBER

by

OGBOLE COLLINS INALEGWU

A THESIS

Presented to the Graduate Faculty of the

MISSOURI UNIVERSITY OF SCIENCE AND TECHNOLOGY

In Partial Fulfillment of the Requirements for the Degree

MASTER OF SCIENCE IN ELECTRICAL ENGINEERING

2021

Approved by:

Dr. Jie Huang, Advisor
Dr. Steve Watkins
Dr. Mina Esmaeelpour

ABSTRACT

Wavelength meters are very important for precision measurements of both pulses and continuous-wave optical sources. Conventional wavelength meters employ gratings, prisms, interferometers, and other wavelength-sensitive materials in their design. Here, we report a simple and compact wavelength meter based on a section of multimode fiber and a camera. The concept is to correlate the multimodal interference pattern (i.e., speckle pattern) at the end-face of a multimode fiber with the wavelength of the input lightsource. Through a series of experiments, specklegrams from the end face of a multimode fiber as captured by a charge-coupled device (CCD) camera were recorded; the images were analyzed using a convolutional neural network (CNN) model for the design of a specklegram wavelength meter. The developed specklegram wavelength meter can accurately map speckle patterns of signature wavelength up to a resolution of 1 pm, which is the operating range of the Hewlett Packard 8168F tunable laser used for the experiment. Furthermore, the incorporated machine learning algorithm of the CNN model can optimally generalize for un-trained categories of a dataset from the same equipment. Up to 150,000 images were captured and utilized to train the CNN over the duration of the experiment. The CNN was trained with several categories of image data sets: from 10 nm, to 1 nm, and progressively down to 1 pm (for selected wavelengths). After training and finetuning, the final output shows 100% classification accuracy for the speckle patterns produced from the design set-up. This shows that a machine learning model can be used for the analysis of specklegrams in the design of a wavelength meter. Also, the developed model can be deployed on modern equipment for wavelength metering at negligible cost.

ACKNOWLEDGMENTS

This thesis is dedicated to my parents: my late dad whose passion for academics inspired this work, and to my mum who has given me the most financial and moral support over the years.

My sincere gratitude to my advisor, Dr. Jie Huang, without whose guidance I would not have been able to complete this research work; his supervision and a great deal of professional insight helped to refine the abstract ideas leading to this final project.

I would like to specially thank my committee members, Dr. Steve Watkins and Dr. Mina Esmaeelpour for their invaluable contributions, Dr. Kurt Kosbar for the opportunity to work under him as a Graduate Teaching Assistant, Dr. Rex Gerald II for the technical and editorial feedback, and the entire faculty and members of staff of the Electrical and Computer Engineering Department.

My most profound appreciation is reserved for my wife, for her love and sacrifices, and for my siblings, my friends, and my colleagues at the Lightwave Technology Laboratory (LTL).

TABLE OF CONTENTS

Page

LIST OF ILLUSTRATIONS

LIST OF TABLES

NOMENCLATURE

Symbol	Description
β	Propagation Constant of travelling wave
ϕ	Phase angle of travelling wave
λ	Wavelength
n	Refractive Index

LIST OF ABBREVIATIONS

Abbreviation	Full Name
MMF	Multimode Fiber
NA	Numerical Aperture
CCD	Charge-Coupled Device
CNN	Convolutional Neural Networks
OPD	Optical Path Difference
IoT	Internet of Things
ReLU	Rectified Linear Unit

1. INTRODUCTION

1.1. BACKROUND

A wavelength meter is a device used to measure the wavelength of a given laser beam. The analysis of wavelength is vital in the signal analysis of pulses and continuous-wave optical sources. This analysis helps researchers and industries to identify the optical characteristics and the state of a product. Signal and optic engineers use a device called the wavelength meter (also called a wavemeter) to carry out accurate wavelength measurements. Wavelength meters are interferometers used specifically for wavelength measurements. A wavelength meter design may employ prisms, gratings, interferometers and other wavelength-sensitive materials as the dispersive elements. For research in the field of optics and the design of optical sensors, the optical fiber is becoming an excellent choice due to its lightweight nature, robustness to the effects of electromagnetic interference, and a capacity for higher bandwidth [1],[2],[3], thus, making it also possible for optical fibers to be used for the design of a wavelength meter. Moreover, the analysis of wavelength is critical for high precision applications in atomic physics, meteorology, and spectrometry [4],[5],[6]. Moreover, since wavelength meters have a vast application in precision measurements, researchers are constantly working on performance improvements through the adoption of various techniques. In [7], the authors caliberated the transmission matrix, this characterizes the spectral-spatial mappings of the optical fiber. In [8], H. Cao further highlights several applications and some challenges. N. Han et al. in [9], adopted the Talbot effect and a tone parameter extraction technique to design a high-precision (with below 10 pm estimation uncertainty) wavelength meter. Some challenges

with the conventional design techniques of measuring wavelengths (i.e., using gratings, prisms, interferometers etc) are: they require ultra-high free space alignment, they are bulky in nature, and they are very expensive. However, due to the sensitivity of optical fibers and their favorable material qualities, they can serve as a dispersive media, replacing conventional bulky and expensive dispersive media elements. In addition, the structure of an optical fiber makes compact designs possible, and they can also be used for a variety of measurements [10],[11].

1.2. BASIC TYPES OF WAVELENGTH METERS

There are many methods employed in the design of wavelength meters: grating wavelength meters [12],[13], optical heterodyne systems [14],[15],[16], and Fabry-Perot interferometry systems [17],[18]. In general, wavelength meters can be classified into two main categories: the scanning wavelength meter and the static wavelength meter. This classification is based on the mode of operation of the device.

1.2.1. Scanning Wavelength Meter. A Scanning wavelength meter is based on the working principle of the Scanning Michelson Interferometer. As depicted in Figure 1.1, the design uses three mirrors, an optical light source, and a detector. The half-silvered mirror acts as a beam splitter, while the other two fully refective mirrors are placed such that one of the mirrors (i.e., the fixed mirror) is directly opposite the light source, and the second mirror (i.e., the movable mirror) is perpendicular to the light source with reference to the beam splitter. The second mirror and the detector are placed opposite each other. During operation, light from the light source hits the beam splitter; the beam splitter will allow one-half of the beam to pass through to the mirror opposite the light source, while the other

half goes to the mirror perpendicular to the light source with reference to the beam splitter. Both beams will rebound and be recombined to give a sinusoidal interference pattern. By varying the distance d, successive fringes are observed (as the beams combine either destructively or constructively). The computation of the wavelength uses the Michelson interferometer equation:

$$m\lambda = 2nd \qquad (1)$$

where m, is the number of fringes observed as the movable mirror is displaced by a distance d, and n is the refractive index of the space, which is typically air.

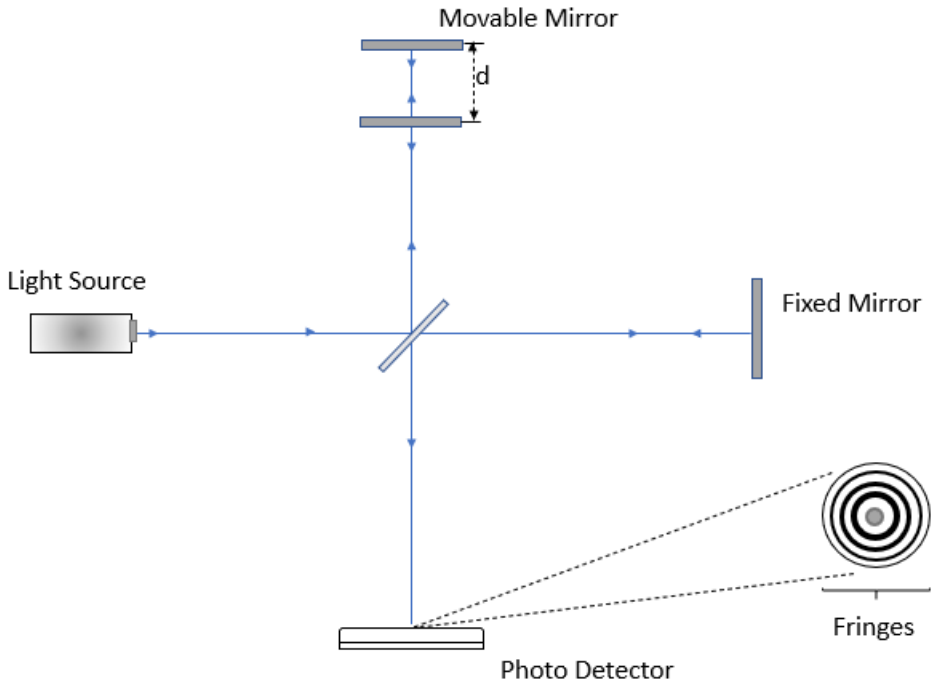

Figure 1.1 Set-up of a Michelson-based Interferometer for Wavelength measurement.

1.2.2. Static Wavelength Meter. Static wavelength meter describes the set of wavelength meters that do not have moving parts. This class of wavelength meters adopts

a solid-state design. An example is the Fizeau interferometer used for wavelength measurements, and can also be used for measuring the surface characteristics of an object. In 1851, Hippolyte Fizeau demonstrated that if a fabricated lens or mirror is compared with another of desired shape (where both mirrors are stacked with a slight angular deviation), the deviation will introduce an optical path difference (OPD) resulting in observable bright and dark fringes. For wavelength measurements, the incident beam is collimated using a collimator. The traveling beams experience interference between the two plano-parallel glass plates as observed in Figure 1.2. This results in parallel fringes observed by a CCD camera. The CCD camera analyzes the period of the fringes and then computes the change in wavelength, that is, from the linear relationship between the change in wavelength (λ) and the period (T) of the light beam travelling at a velocity (v) as shown in Equation 2.

$$T = \frac{\lambda}{\mathrm{v}} \qquad (2)$$

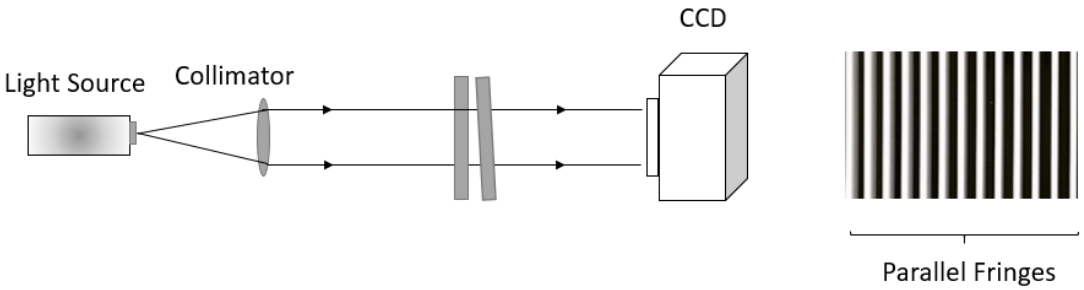

Figure 1.2 Set-up of a Fizeau-based Interferometer for Wavelength measurement.

1.3. MULTIMODE FIBER SPECKLEGRAM

In both the Michelson and Fizeau Interferometer, fringes are generated because of constructive and destructive interference of traveling optical waves. When the interference of the incident beams is in phase, the resulting effect on successive fringes is a bright ring

shape, while a dark ring shape corresponds to a destructive (i.e., out of phase) interference for the Michelson Interferometer, while for the Fizeau Interferometer, successive parallel fringes are observed. The traditional wavelength meters may yield very high accuracy of up to 0.1 pm (an example is the Bristol Instrument), however, they are limited by the need for ultra high free space alignment, the bulky nature of the optical elements, and high cost. Consequently, researchers are turning towards light-weight and compact materials like optical fibers. As an optical dispersive element, when light is propagated through a multimode fiber (MMF), there will also be observable constructive and destructive interferences. The different modes interfere both constructively and destructively to produce corresponding bright and dark spots called specklegrams or speckle patterns, as depicted in Figure 1.3.

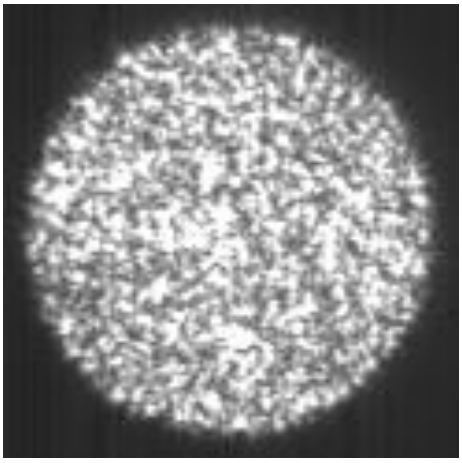

Figure 1.3 A specklegram image at the end facet of a multimode fiber.

The generated speckle pattern can be investigated for wavelength measurements because it is unique to each wavelength, so long as the set-up remains unchanged [19].

1.4. RESEARCH OBJECTIVES

The aim of this thesis is to design a simple and compact wavelength meter that adopts a solid-state design. The proposed design method will analyze specklegrams generated by propagated light through a multimode fiber using machine learning. The following are the design objectives:

1. To understand the underlying relationship between a speckle pattern (specklegram) and its signature wavelength.
2. To develop and train a machine learning model that can accurately identify a given wavelength from its signature splecklegram.
3. To test the developed model on several categories of data sets (specklegram images).
4. To develop a low-cost wavelength meter.

1.5. THESIS OVERVIEW

The aim of this project is to produce a low-cost wavelength meter using a multimode fiber (MMF) by correlating the multimodal interference pattern (i.e., specklegram or speckle pattern) at the end face of the multimode fiber with the wavelength of the input light source. The design adopts a machine learning model for the analysis of the specklegrams.

Section 2 focused on the review of literature and the applications of the specklegram concept for the development of a wavelength meter and for other measurement and sensing applications.

Section 3 presents the methodology and experimental set up. This section provides details on the data collection, data processing, and the architecture of the desired machine learning model (i.e., the convolutional neural network).

Section 4 provides details of the result from the training and testing of the convolutional neural network (CNN) model. This section also shows comparison with results from other pretrained machine learning models. Further discussion of the results is presented in this section.

Section 5 gives a summarized conclusion and recommendation for future works.

2. LITERATURE REVIEW

2.1. MULTIMODE FIBER (MMF) SPECKLEGRAM DESIGN

B. Redding and H. Cao in [19] proposed and demonstrated that using a MMF as a dispersive media, the propagated light produces speckle patterns that are a signature of the wavelength of the input signal. Redding et al. in [20] showed how a MMF is used as a standard spectrometer. Furthermore in [21], they showed how this architecture — using a MMF and a charge-coupled device (CCD) camera — can be used to reconstruct speckle patterns for an all-fiber spectrometer using a transition matrix. The transition matrix served as a fingerprint that uniquely identified an input wavelength. Liew et al. in [22] achieved a resolution of 1 pm at a wavelength of 1500 nm. However, the model was limited in the ease of adaptability over a dynamic range of wavelengths and varying environmental conditions. Furthermore, by speckle pattern analysis using a stabilized diode laser source and a disordered medium to scatter the light, the authors in [23] were able to realize attometer resolution using principal component analysis to detect the wavelength changes of a stabilized laser diode. Therefore, it is evident that the concept of speckle pattern analysis has led to a variety of breakthroughs in optical sensing. Some example applications are: chemical specklegram sensor [24], where a concatenated multimode-no-core-multimode structure was used for detecting various liquid samples. Force myography sensor [25], where a transducer was attached to the forearm of the user, and the change in specklegram with the movement of the hand was captured and referenced with calibration positions. Furthermore, the authors in [26] presented a review of specklegram modal modulated sensors, and temperature and weight measurement sensors were developed in

[27]. Also, sensing of fluid properties, and mechanical stimuli were investigated in [28] and [29], respectively. All these research efforts support the fact that multimode fibers exhibit predictable behavior, which can be exploited for use in wavelength meter development [30].

The advancement in technology has led to the use of machine learning as a powerful tool for imaging and computer vision analysis. In machine learning, a user tries to imitate the way humans learn through sets of collected data and algorithms; it then trains a model to understand these patterns and to improve on the accuracy. Machine learning has been applied to optical sensors in many recent research efforts: fiber directional position sensors [31], classification and reconstruction of handwritten digits [32], multifunctional optical spectrum analysis [33], material science [34], holographic microscopy [35], structural health monitoring [36], speckle wavemeter using a disordered medium[35], fiber optic sensor embedded smart helmet [37], and pecklegram sensors for mechanical measurements [38]. The machine learning models are able to learn the underlying relationships between the trained dataset and the expected output(s), and in most cases the models show superiority over the traditional statistical signal processing approaches [39].

2.2. BENEFITS OF FIBER SPEKLEGRAM DESIGNS

Discussed earlier are some of the applications of the fiber specklegram designs. This area of research has seen several applications within the last two decades due to its tremendous benefits, some of which are listed below:

i. The designs do not require costly interrogation equipment (only use a laser source and a CCD camera).

ii. High measurement resolutions in sensing applications due to the highly sensitive nature of specklegram designs.

iii. Specklegram designs can be used to achieve multiplexing capabilities by varying the physical orientation of the design set up, or by making changes to the wavelength of the incident light source.

iv. With the growing trend in machine learning for image processing, remote sensing, and internet of things (IoT), specklegram designs show enormous potential for the general improvement in fiber sensor applications,

2.3. CHALLENGES OF FIBER SPEKLEGRAM DESIGNS

Specklegram designs come with challenges as well. Listed below are some of the challenges:

i. Extra packaging is required to ensure stability against the influence of mechanical perturbation, due to the highly sensitive nature of optical fibers.

ii. The set-up of the design has to be maintained for a given sensing application because the sensing ability is highly dependent on the optical fiber's parameters. Some of the parameters that can result to variations in an optical fiber sensor are: the length of the fiber, the dimension of the core, the numerical aperture (NA) etc.

3. METHODOLOGY AND EXPERIMENTAL SET-UP

3.1. METHODOLOGY

Speckle patterns are stochastically spatially distributed. Therefore, traditional analyses of their nature always employ statistical signal processing tools [40],[38]. For a mean value of the speckle pattern with intensity I, the probability density function can be expressed as:

$$p(I) = \frac{I}{\langle I \rangle} \exp\left(\frac{-I}{\langle I \rangle}\right) I \tag{3}$$

Also, the travelling modes in the fiber core could either interfere constructively or destructively, resulting in the observation of speckle patterns. Although, it is numerically possible to differentiate the speckle patterns of wavelength values farther apart, it becomes very complex to do so for closely separated wavelength values. For this reason, a machine learning algorithm was determined to be best suited for this task. Since a shift in the wavelength results in a corresponding change in each guided mode's propagation constant (β_m, where m is for the mth guided mode) and its phase delay ($\emptyset_m$, also for the mth mode as well), the expression for the propagation constant is given by Equation 4:

$$\Delta\beta_m = \beta_m(\lambda + \Delta\lambda) - \beta_m(\lambda) \tag{4}$$

and the change in the phase is expressed for a given length (L) is expressed as:

$$\Delta\emptyset_m = \Delta\beta_m L \tag{5}$$

Because these changes are a function of the length (L) of the fiber, it is evident that the changes in speckle patterns are easily noticed in longer fibers. Thus, in [19] it was reported that a 1 m long MMF achieved a spectral resolution of 0.15 nm while a 5 m long MMF resolved a spectral resolution of 0.03 nm, using the transmission matrix method; both cases were over a bandwidth of 25 nm and 5 nm, respectively. Also, in [7] we see that the authors used a 100 m multimode fiber to be able to achieve 1 pm resolution with a similar set up. Therefore, depending on the resolution of the light source, it is possible to achieve beyond picometer resolution. And for a a multimode fiber with a large core diameter, more modes will be excited and accommodated along the length of the fiber, leading to the observation of more speckles.

3.2. DATA ACQUISITION

For the experimental set-up, a Hewlett Packard 8168F (operating at 1440 nm to 1590 nm wavelength range with a 1 pm resolution) tunable laser source was used as the input light source. A commercially available 16 m long step-index MMF (core diameter = 400 μm, NA = 0.48) was coupled to the tunable laser source to serve as the dispersive element, resulting in the multimode interference speckle patterns along the core of the fiber. The MMF was coiled so that it can remain imobilized within the set-up space while the experiment was being conducted — to ensure a controlled structure. Figure 2.1 shows the schematic of the entire set up.

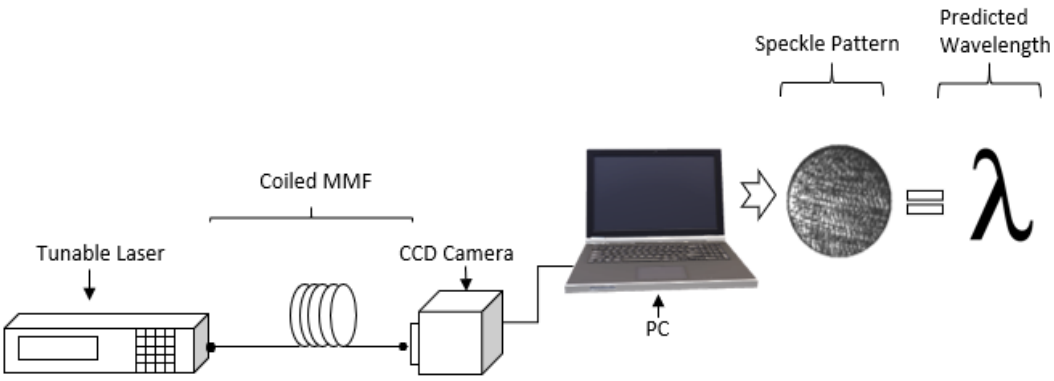

Figure 3.1 Schematic of the Set-up

The Tunable Laser source is used to transmit light of a selected wavelengt through the MMF, while the CCD camera is used to capture the speckle pattern at the end face. The captured speckle pattern is saved to the PC and processed for further analysis. Figure 3.1 shows one end of the MMF connected to the Tunable Laser source, and its distal end securely placed before the CCD camera. The image at the end face is captured by the camera. Image acquisitions were first carried out for the entire wavelength range (1440 nm to 1590 nm) in steps of 10 nm. For each step, 1000 images were captured. Afterwards, smaller resolutions with 1 nm, 0.1 nm, 0.01 nm and finally 0.001 nm (1 pm) step sizes were captured — 0.001 nm was the smallest step size the tunable laser could achieve. For the 1 pm step sizes in wavelength change, the captured images were recorded at 1500 nm; the decision to work at this wavelength was because it is at the middle operational range, and a 1 pm step size would result in millions of speckle images to analyze if adopted for the entire operational range of the equipment. However, to test if the CNN model can accurately generalize across the entire wavelength range of the device, similar data was collected at 1440 nm – 1449 nm and at 1580 – 1590 nm, respectively (both ranges are at

the operational end ranges of the Tunable Laser source). For the entire time of the experiment, over 150,000 images were captured and labelled; care was taken to avoid effects of environmental perturbation by using the fiber optic table for every set of images captured. Figure 3.2 shows some of the speckle patterns captured at different wavelengths (step sizes of 100 pm and 1 pm).

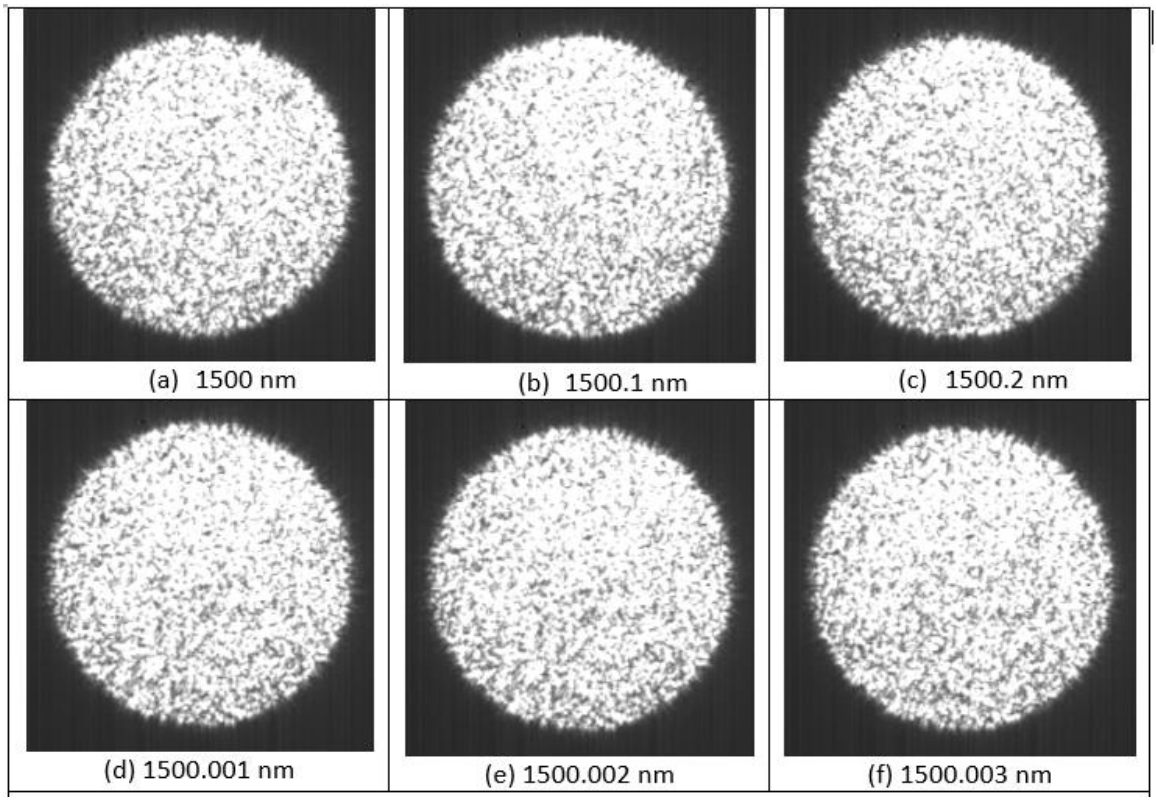

Figure 3.2 Specklegram images (a) – (c) are at a step sizes of 100pm and (d) – (f) at 1 pm.

Figure 3.2 clearly shows that the speckle patterns become extremely difficult to distinguish by the naked eyes (some even undistinguishable) with smaller wavelength increments.

3.3. THE CNN MODEL

By observing the images in Figure 3.2, it is evident that closely resolved speckle images were very similar in appearance and difficult to differentiate when dealing with an increasing number of images. For this reason, a CNN model was developed to understand the underlying correlations and to accurately map a speckle pattern to its signature wavelength. The model used has a summarize structure shown in Table 3.1.

Table 3.1 CNN Model Summary

Layers	Type	Kernel/Pool Sizes	Activation Function
1	Convolution2D_1 Maxpooling2D_1	Kernel size = 3x3 Pool size = 2x2	ReLU -
2	Convolution2D_2 Maxpooling2D_2	Kernel size = 3x3 Pool size = 2x2	ReLU -
3	Flatten	-	-
4	Dense_1	-	ReLU
5	Dense_2(with Dropout)		-
6	Dense_3		Softmax

The model as depicted in Table 3.1 has six layers with their functions stated below.

3.3.1. The Convolutional Layer. The convolutional layer is the first layer for the extraction of features of the input images. Convolution is the mathematical linear operation where a dot product function is obtained from the multiplication of two other functions. This product function expresses how the shape of the first function is affected by that of

the second function. These functions are expressed in matrix form, where the first function is the input image matrix of size M x M, and the second is that of the filter of size N x N. The final output term resulting from sliding the filter over the input image is called the feature map. The feature map contains information about the edges of the input image.

3.3.2. Pooling Layer. The pooling layer follows the convolutional layer, and it has the primary aim of decreasing the size of the feature map obtained from the convolutional layer. The goal was to reduce the computational cost. Some pooling methods are the max pooling; this takes the largest element from each pool (i.e., if it is a 2x2 pooling size, it will take the element with the highest value from each pool size), and combines them to form a reduced feature map. The average pooling computes the average value of the elements, and the sum pooling uses the value of the sum of the elements**.**

3.3.3. Flatten Layer. The flatten layer organizes the pooled feature map into a single column vector. This was achieved by taking the row-by-row values of the pooled feature map and making them a 1-dimensional feature vector to be used by the dense layer.

3.3.4. Dense layer. In this layer, each neuron received an input from all the neurons of the previous layer (i.e., the flatten layer). The operation of this layer was to perform a dot multiplication of the input values (x) and the weight (w) presented to it for obtaining the output classes (Y). However, the end result has to pass through the activation function (f) to yield an output, expressed as:

$$Y = f(w * x + b) \tag{6}$$

where b, is a bias term.

3.3.5. Dropout Layer. The function of the dropout was to check against overfitting. Overfitting is a situation where a particular model is only able to perform

perfectly well on the training set (seen data), however, it performs poorly on the test set (unseen data). It happens when the model memorizes the seen data and fails to understand the underlying relationship — this makes it unable to generalize for unseen data. A solution to this is to randomly drop some neurons during the training process, which is what the dropout achieves.

3.3.6. Activation Function. Activation functions are used to approximate complex relationships between variables. The activation function helps to add non-linearity to the network. Some common examples are the Rectified Linear Unit (ReLU) function, Sigmoid function, Softmax etc. Every activation function has its specific usage. For example, the sigmoid function is a good choice for binary classification, while the softmax is preferred for multi-class classification problems.

In summary, the developed model has its first two layers as a series of convolutions and pooling with kernel sizes 3x3 and pool size 2x2, respectively. The convolution unit on both layers uses the Rectified Linear Unit (ReLU) activation function. The ReLU function does not update all neurons at the same time, therefore, the positive portion is updated more rapidly during training; this helps to speed up the process. Next is the Flatten layer, which converted the data to a 1-dimensional array feature vector, and it was followed by a dense layer that performed the matrix-vector multiplication, and adopted a ReLU activation function. After the flatten layer, there was another dense layer with a dropout function to prevent the model from overfitting. Finally, there was a third dense layer with a softmax activation function for the classification. The CNN model was developed on the Jupyter notebook within the Anaconda software package. The Anaconda package is an open-source platform for Python data science computation, and the design utilized the Keras API

running on Windows 10 and TensorFlow back end. The choice of this package prevailed because it was user friendly, and it came with many other development tools for data science analyses.

4. EXPERIMENTAL RESULT AND DISCUSSION

4.1. RESULT WITH TRAINED CATEGORY OF DATASET

Several cases were tested, with the first set of training on speckle patterns at 10 nm steps apart. Since this was the first case analyzed, major tuning of the model's hyperparameters was made at this stage. After several trials and finetuning of the parameters, a model with a learning-rate = 0.001, batch size = 20, and beta value = 0.9 was shown to achieve an accuracy of 100% at this step size. The data set had 9,000 images of which 8,000 images were used for training (with validation split = 0.15), and the remaining 1,000 images for testing of the model. This model was then deployed for the next set of cases with step sizes of 1 nm, 0.1 nm, 0.01 nm, and 0.001 nm (1 pm), respectively. For each of these cases, 8,000 images were used for training and 1,000 were used to test the model.

Typically, the images were first converted to arrays with pixel values in the range [0, 255] before being fed to the network as shown in Figure 4.1.

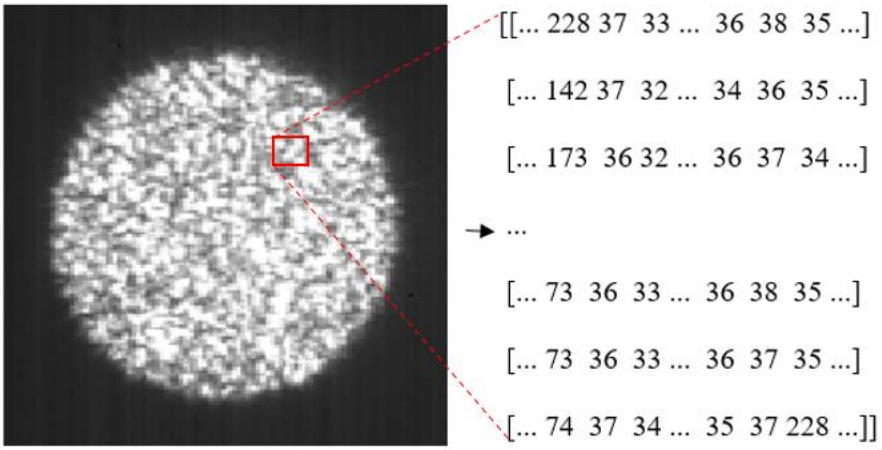

Figure 4.1 Specklegram as a matrix of pixel values.

Figure 4.1 shows a 256 x 256 matrices of the intensity distribution, with the value 255 denoting a pixel with the most intensity (regions where the interference is in phase), and 0 denoting a pixel with the least intensity (region where the interference is completely out of phase). After several training iterations (with modifications to the hyperparameters), an accuracy of 100% was still achieved with the developed model. Table 4.1 further shows the result for the CNN model adopted for the classification task. In addition, VGG16 and RESNET50, both award winning models for image classification challenges were also tried on this data set — basically to see how well the pretrained models will perform on this dataset without any tweaking of parameters. Table 4.1 shows the computed result for the 1 pm step size analysis. The networks were fed with a balanced data set, with all classes having equal number of images for the training and testing of the model. If this balance was not maintained, the classifier was very likely to be bias, thus, leading to overfitting for the more represented class.

Table 4.1 Training and Test Results for the Different Models

Step Size	Model	Number of Images		Accuracy (%)	
		Trained (Validation Split = 0.15)	Test	Train	Test
1 pm	Used-Model	8,000	1,000	100	100
1 pm	VGG16	8,000	1,000	96.1	74.5
1 pm	RESNET50	8,000	1,000	91.2	67.4

The grouped bar chart in Figure 4.2 further captures the summary of the training and test results. Just like the table, the bar chart also shows the accuracy result at 1 pm for the testing and training for all three models. The Used-Model showed 100% classification accuracy at both training and testing stages.

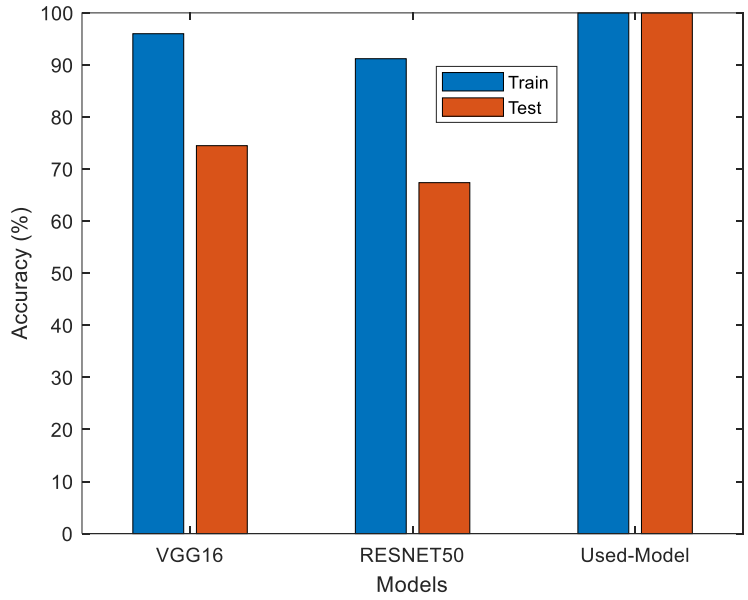

Figure 4.2 Training and Test Result for VGG16, RESNET50 and Used-Model.

4.2. RESULTS WITH UNTRAINED CATEGORY OF DATASET

To further test the generalization of the developed model, a new category of completely untrained images was analyzed. The analysis of the new category of data set yielded 100% accuracy. It is worth noting that the set of testing with an untrained range of wavelengths took a longer time to converge; however, it still achieved 100% accuracy as seen in Figure 4.3.

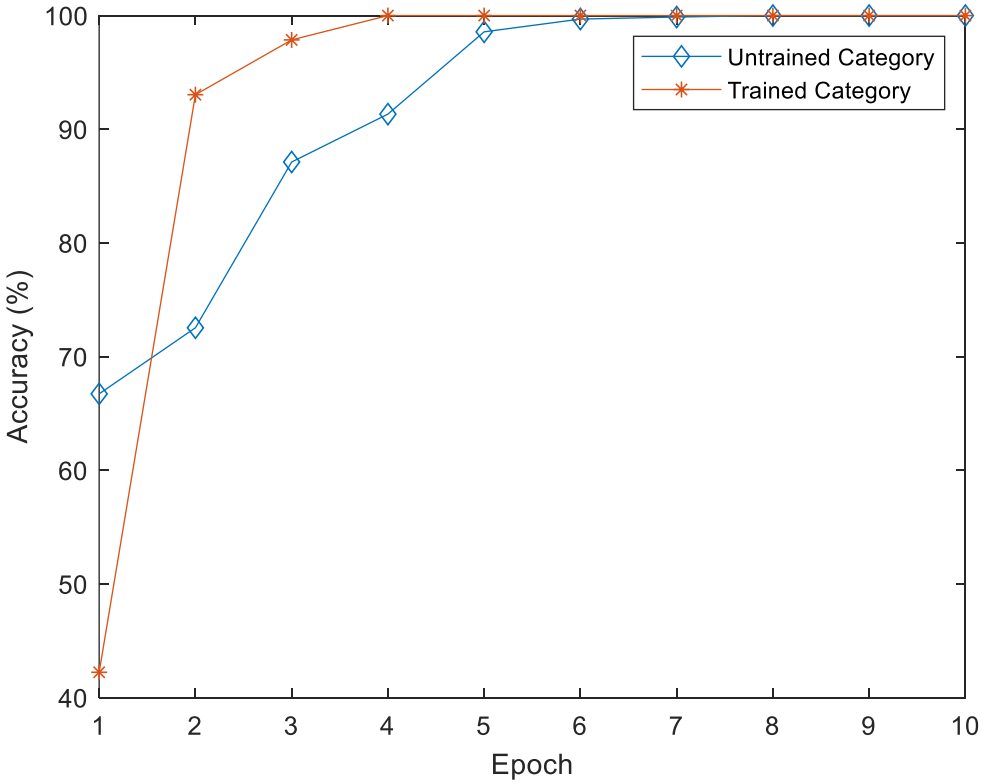

Figure 4.3 Trained and Untrained Data Accuracy at Different Epochs.

With the trained category, optimum accuracy was achieved at an earlier epoch as compared with the untrained category: for the trained set, an accuracy of 100% was achieved by the 4th epoch. For the category of untrained data, it was at the 8th epoch that 100% accuracy was achieved. From the results presented above, speckle-based wavemeters are effective for accurately classifying narrowly resolved wavelengths using machine learning. Although, it may take some time to develop an effective and efficient model, once a working model has been developed, it becomes easy to adapt, making it a scalable approach. For example, Figure 4.2 showed results for two pretrained models, VGG16 and RESNET50; both models performed well without modifications to the hyperparameters. Some modifications made to the data set were in the image dimensions, where all images

were set to 256x256 pixels for uniformity. Also, the dark background was cropped out as part of the preprocessing steps for some cases; it was noticed that this did not significantly affect the training and test result. The datasets fed for training were all shuffled and each image had its unique identification as a ground truth label. For the 1 pm resolved speckle patterns, the model must rely entirely on other underlying features such as the spatial distribution of the spots for each wavelength.

In conclusion, the analysis of speckle patterns require advance tools beside traditional computational methods for accurate processing, and a CNN algorithm was ideal for this task.

The goal of using the optical table for the set up was to ensure that the initial conditions of the experiment were maintained all through the various data collection periods. Noteworthy, was the effect of vibration on the set up: to examine if there would be any instability resulting from external vibrations, the set-up was intentionally forced to vibrate. The outcome from the forced vibration was recorded, and it showed that the speckle orientation for a given set of parameters (i.e., the specific wavelength and the environmental condition at the given time) would always return to its initial orientation in about 3 – 5secs after the applied force was removed.

5. CONCLUSION AND FUTURE WORKS

This work demonstrated that it is possible to accurately classify all possible resolved wavelengths from their signature speckle patterns. The experiment used a tunable laser as the light source, and a convolutional neural network model for data analyses. Furthermore, the work was compared with results from existing pretrained models (VGG16 and RESNET50); the outcomes validated the power of machine learning in this area of study. A concern during the process of data collection was environmental influence, since the speckles are extremely sensitive to physical perturbation from the surrounding environment. To check the effect of environmental perturbation, it was very important to have the data captured on a stable stage. For the work reported herein, an optical table was used. This method of wavelength prediction is cheap and adaptable, and uses a multimode fiber, a CCD camera and a 16G RAM, core i7 Dell PC. Moreover, with this simple setup, the method can be easily incorporated into digital mobile devices, and the developed CNN model can be further utilized for untrained data sets for the design of a simple and compact wavelength meter. The transfer learning ability of the model makes it easily deployable and adaptable to a wide range of wavemeter applications.

All data collected for this work was at room temperature. Future work will consider the inclusion of a temperature controller, since the device is temperature sensitive. Also, the application of speckle patterns towards sensing of other physical parameters besides wavelength measurements will be investigated.

BIBLIOGRAPHY

[1] A. Güemes, A. Fernández-López, and B. Soller, “Optical Fiber Distributed Sensing - Physical Principles and Applications,” Struct. Heal. Monit., vol. 9, no. 3, pp. 233–245, May 2010, doi: 10.1177/1475921710365263.

[2] S. Pevec and D. Donlagic, “Miniature fiber-optic sensor for simultaneous measurement of pressure and refractive index,” Opt. Lett., vol. 39, no. 21, p. 6221, Nov. 2014, doi: 10.1364/OL.39.006221.

[3] C. Zhu, D. Alla, and J. Huang, “High-temperature stable FBGs fabricated by a point-by-point femtosecond laser inscription for multi-parameter sensing,” OSA Contin., vol. 4, no. 2, p. 355, Feb. 2021, doi: 10.1364/OSAC.415685.

[4] M. Ghadimi et al., “Multichannel optomechanical switch and locking system for wavemeters,” Appl. Opt., vol. 59, no. 17, p. 5136, Jun. 2020, doi: 10.1364/AO.390881.

[5] J. D. White and R. E. Scholten, “Compact diffraction grating laser wavemeter with sub-picometer accuracy and picowatt sensitivity using a webcam imaging sensor,” Rev. Sci. Instrum., vol. 83, no. 11, p. 113104, Nov. 2012, doi: 10.1063/1.4765744.

[6] T. Wang, Y. Li, B. Xu, B. Mao, Y. Qiu, and Y. Meng, “High-resolution wavemeter based on polarization modulation of fiber speckles,” APL Photonics, vol. 5, no. 12, p. 126101, Dec. 2020, doi: 10.1063/5.0028788.

[7] B. Redding, M. Alam, M. Seifert, and H. Cao, “High-resolution and broadband all-fiber spectrometers,” Optica, vol. 1, no. 3, p. 175, Sep. 2014, doi: 10.1364/OPTICA.1.000175.

[8] H. Cao, “Perspective on speckle spectrometers,” J. Opt., vol. 19, no. 6, p. 060402, Jun. 2017, doi: 10.1088/2040-8986/aa7251.

[9] N. Han, G. N. West, A. H. Atabaki, D. Burghoff, and R. J. Ram, “Compact and high-precision wavemeters using the Talbot effect and signal processing,” Opt. Lett., vol. 44, no. 17, p. 4187, Sep. 2019, doi: 10.1364/OL.44.004187.

[10] P. J. Winzer, “Scaling Optical Fiber Networks: Challenges and Solutions,” Opt. Photonics News, vol. 26, no. 3, p. 28, Mar. 2015, doi: 10.1364/OPN.26.3.000028.

[11] M. Roman, C. Zhu, R. J. O’Malley, R. E. Gerald, and J. Huang, “Distributed Fiber-Optic Sensing With Low Bending Loss Based on Thin-Core Fiber,” IEEE Sens. J., vol. 21, no. 6, pp. 7672–7680, Mar. 2021, doi: 10.1109/JSEN.2021.3050702.

[12] F. J. Duarte, “Prism-grating system for laser wavelength measurements,” J. Phys. E., vol. 16, no. 7, pp. 599–601, Jul. 1983, doi: 10.1088/0022-3735/16/7/006.

[13] C. Wei, S. Yan, and T. Zhang, “Compact diffraction grating laser wavemeter for cold atom experiments,” Optoelectron. Lett., vol. 13, no. 5, pp. 335–338, Sep. 2017, doi: 10.1007/s11801-017-7092-8.

[14] X. Wang, Y. Li, and S. Zhang, “Heterodyne wavelength meter for continuous-wave lasers,” Appl. Opt., vol. 46, no. 23, p. 5631, Aug. 2007, doi: 10.1364/AO.46.005631.

[15] H. Hussein, M. A. Sobee, and M. Amer, “Calibration of a Michelson-type laser wavemeter and evaluation of its accuracy,” Opt. Lasers Eng., vol. 48, no. 3, pp. 393–397, Mar. 2010, doi: 10.1016/j.optlaseng.2009.10.002.

[16] Y. Xiao, S. Sun, W. Li, N. Zhu, and M. Li, “Ultra-Fast Wavemeter for CW Laser Based on Wavelength-to-Time Mapping,” J. Light. Technol., vol. 37, no. 11, pp. 2661–2667, Jun. 2019, doi: 10.1109/JLT.2018.2882909.

[17] A. Fischer, R. Kullmer, and W. Demtröder, “Computer controlled Fabry-Perot wavemeter,” Opt. Commun., vol. 39, no. 5, pp. 277–282, Nov. 1981, doi: 10.1016/0030-4018(81)90091-2.

[18] J. H. Goad, Jr., “Construction And Performance Of A Fabry-Perot Inteferometer Based Airborne Autonomous Wavemeter For Laser Tuning,” Apr. 1990, p. 360, doi: 10.1117/12.962762.

[19] B. Redding and H. Cao, “Using a multimode fiber as a high-resolution, low-loss spectrometer,” Opt. Lett., vol. 37, no. 16, p. 3384, Aug. 2012, doi: 10.1364/OL.37.003384.

[20] B. Redding, S. M. Popoff, and H. Cao, “All-fiber spectrometer based on speckle pattern reconstruction,” Opt. Express, vol. 21, no. 5, p. 6584, Mar. 2013, doi: 10.1364/OE.21.006584.

[21] B. Redding, S. M. Popoff, Y. Bromberg, M. A. Choma, and H. Cao, “Noise analysis of spectrometers based on speckle pattern reconstruction,” Appl. Opt., vol. 53, no. 3, p. 410, Jan. 2014, doi: 10.1364/AO.53.000410.

[22] S. F. Liew, B. Redding, M. A. Choma, H. D. Tagare, and H. Cao, “Broadband multimode fiber spectrometer,” Opt. Lett., vol. 41, no. 9, p. 2029, May 2016, doi: 10.1364/OL.41.002029.

[23] G. D. Bruce, L. O’Donnell, M. Chen, and K. Dholakia, “Overcoming the speckle correlation limit to achieve a fiber wavemeter with attometer resolution,” Opt. Lett., vol. 44, no. 6, p. 1367, Mar. 2019, doi: 10.1364/OL.44.001367.

[24] E. Fujiwara, L. E. da Silva, T. D. Cabral, H. E. de Freitas, Y. T. Wu, and C. M. de B. Cordeiro, “Optical Fiber Specklegram Chemical Sensor Based on a Concatenated Multimode Fiber Structure,” J. Light. Technol., vol. 37, no. 19, pp. 5041–5047, Oct. 2019, doi: 10.1109/JLT.2019.2927332.

[25] E. Fujiwara, Y. T. Wu, M. F. M. Santos, E. A. Schenkel, and C. K. Suzuki, “Identification of hand postures by force myography using an optical fiber specklegram sensor,” Sep. 2015, p. 96343Z, doi: 10.1117/12.2194605.

[26] H. S. Efendioglu, “A Review of Fiber-Optic Modal Modulated Sensors: Specklegram and Modal Power Distribution Sensing,” IEEE Sens. J., vol. 17, no. 7, pp. 2055–2064, Apr. 2017, doi: 10.1109/JSEN.2017.2658683.

[27] and Y.-Q. L. Jiao-Jiao Wang, Shao-Cheng Yan, Ya-Ping Ruan, Fei Xu, “Fiber-Optic Point-Based Sensor Using Specklegram Measurement,” Sensors, vol. 17, no. 10, p. 2429, Oct. 2017, doi: 10.3390/s17102429.

[28] T. D. Cabral, E. Fujiwara, S. C. Warren-Smith, H. Ebendorff-Heidepriem, and C. M. B. Cordeiro, "Multimode exposed core fiber specklegram sensor," Opt. Lett., vol. 45, no. 12, p. 3212, Jun. 2020, doi: 10.1364/OL.391812.

[29] E. Fujiwara, Y. Ri, Y. T. Wu, H. Fujimoto, and C. K. Suzuki, "Evaluation of image matching techniques for optical fiber specklegram sensor analysis," Appl. Opt., vol. 57, no. 33, p. 9845, Nov. 2018, doi: 10.1364/AO.57.009845.

[30] M. Plöschner, T. Tyc, and T. Čižmár, "Seeing through chaos in multimode fibres," Nat. Photonics, vol. 9, no. 8, pp. 529–535, Aug. 2015, doi: 10.1038/nphoton.2015.112.

[31] K. Sun, Z. Ding, and Z. Zhang, "Fiber directional position sensor based on multimode interference imaging and machine learning," Appl. Opt., vol. 59, no. 19, p. 5745, Jul. 2020, doi: 10.1364/AO.394280.

[32] N. Borhani, E. Kakkava, C. Moser, and D. Psaltis, "Learning to see through multimode fibers," Optica, vol. 5, no. 8, p. 960, Aug. 2018, doi: 10.1364/OPTICA.5.000960.

[33] D. Wang et al., "Machine Learning-Based Multifunctional Optical Spectrum Analysis Technique," IEEE Access, vol. 7, pp. 19726–19737, 2019, doi: 10.1109/ACCESS.2019.2895409.

[34] H. S. Stein, D. Guevarra, P. F. Newhouse, E. Soedarmadji, and J. M. Gregoire, "Machine learning of optical properties of materials – predicting spectra from images and images from spectra," Chem. Sci., vol. 10, no. 1, pp. 47–55, 2019, doi: 10.1039/C8SC03077D.

[35] T. Pitkäaho, A. Manninen, and T. J. Naughton, "Focus prediction in digital holographic microscopy using deep convolutional neural networks," Appl. Opt., vol. 58, no. 5, p. A202, Feb. 2019, doi: 10.1364/AO.58.00A202.

[36] S. Li and L. Sun, "Detectability of Bridge-Structural Damage Based on Fiber-Optic Sensing through Deep-Convolutional Neural Networks," J. Bridg. Eng., vol. 25, no. 4, p. 04020012, Apr. 2020, doi: 10.1061/(ASCE)BE.1943-5592.0001531.

[37] Y. Zhuang et al., “Fiber optic sensor embedded smart helmet for real-time impact sensing and analysis through machine learning,” J. Neurosci. Methods, vol. 351, p. 109073, Mar. 2021, doi: 10.1016/j.jneumeth.2021.109073.

[38] A. G. Leal-Junior, A. Frizera, C. Marques, and M. J. Pontes, “Optical Fiber Specklegram Sensors for Mechanical Measurements: A Review,” IEEE Sens. J., vol. 20, no. 2, pp. 569–576, Jan. 2020, doi: 10.1109/JSEN.2019.2944906.

[39] S. Haykin, “Neural networks expand SP’s horizons,” IEEE Signal Process. Mag., vol. 13, no. 2, pp. 24–49, Mar. 1996, doi: 10.1109/79.487040.

[40] S. Wu, S. Yin, and F. T. S. Yu, “Sensing with fiber specklegrams,” Appl. Opt., vol. 30, no. 31, p. 4468, Nov. 1991, doi: 10.1364/AO.30.004468.

VITA

Ogbole Collins Inalegwu was born in Benue, Nigeria. He received his bachelor's degree from Federal University of Technology Minna, Nigeria, in February 2011.

In Summer 2019, he joined the graduate program in the Department of Electrical and Computer Engineering at Missouri University of Science and Technology, under the guidance of Dr. Jie Huang. His research interests included fiber optic sensors and machine learning.

In December 2021, he received his master's degree in the Department of Electrical and Computer Engineering from Missouri University of Science and Technology.